Environ. Sci. Technol. 1987, 21, 178–182

Isoaxial Aerosol Sampling: Nondimensional Representation of Overall Sampling Efficiency

Ken Okazaki,† Russell W. Wiener, and Klaus Willeke*

Aerosol Research Laboratory, Department of Environmental Health, University of Cincinnati, Cincinnati, Ohio 45267-0056

■ Accurate aerosol measurements of ambient and industrial air environments are essential for the protection of human health. In this study, the overall aerosol sampling efficiency of a tubular thin-walled inlet, sampling isoaxially from environmental airflows, has been determined by a dynamic evaluation technique for various values of particle size, wind and inlet velocities, and inlet size. With the assumption of laminar flow, models developed from the results discriminate the dominant mechanisms that modify the sample properties during sampling and evaluate quantitatively the possible sampling errors for relatively wide ranges of sampling conditions. For Stokes numbers less than 0.03, the sampling efficiencies are 100 ± 20%, while for Stokes numbers larger than about 0.3 particle losses in the inlet become significant. On the basis of a large number of experimental data, the overall sampling efficiency of the inlet has been described accurately by a new nondimensional parameter consisting of Stokes number, gravitational deposition parameter, and Reynolds number.

Introduction

When aerosols are sampled from ambient or industrial environments, air with particles suspended in it is drawn through an inlet to a filter or direct-reading instrument. It is essential that the sampled aerosol be representative of the aerosol upstream of the sampler; i.e., the aerosol concentration, size distribution, chemistry, and other properties should be unchanged by the sampling process. If changes do occur, they should be known or predicted quantitatively to the greatest extent possible.

Particles above a few micrometers in aerodynamic diameter may deviate from the air streamlines as they bend toward the inlet face. This results in a change in particle concentration and size distribution of the sampled aerosol. Most of the theoretical and experimental studies have focused on this aspiration process (*1–13*). In addition to aspiration, particle losses by gravitational deposition and impaction on the inner wall of the inlet may also change the sample properties. Thus, the overall sampling efficiency is generally lower than the sampling efficiency based on aspiration alone. Previous studies considering the entire inlet have primarily evaluated specific inlet designs (*14–22*). The purpose of this study was to develop a comprehensive and generalized model for evaluating the aerosol sampling accuracy for a wide range of conditions. Laminar flow conditions are assumed throughout the study. The effect of turbulence is currently under investigation and will be reported on at a later time.

Our initial studies (*23*, *24*) dealt with results and interpretations for an inlet of a specific size. We have now performed a large amount of systematic experiments utilizing different sizes of tubular thin-walled and sharp-edged inlets in our horizontal wind tunnel. Various factors were found to affect the overall sampling efficiency. The results have been modeled to discriminate the dominant mechanisms that modify the properties of the sample depending on the Stokes number range of the sampled particle. In this paper, we discuss our findings for isoaxial sampling where the inlet is aligned parallel to the wind direction. Our findings for non-isoaxial sampling will be described in a separate paper.

Experimental Procedures

Our wind tunnel setup (*23*) has been computerized for fast data acquisition and manipulation of our sampling efficiency data. Test aerosols of oleic acid are generated by a specially designed vibrating-orifice aerosol generator (*25*, *26*) and are homogeneously dispersed into the air flow (*23*). The sampling inlet in the test section of the wind tunnel is integrated into the sensor of an optical single-particle counter that has been further modified so as to accomodate a high flow rate for the larger inlet sizes. The sampling inlet is surrounded by clean sheath air so that all aerosol particles that have passed through the inlet tube are registered by the sensor. All inlets used have been designed to be thin walled and sharp edged so as to meet the inlet design criteria of Belyaev and Levin (*6*, *7*), which require the ratio of the exterior diameter to the interior diameter of the inlet face to be ≤1.05 and the angle of taper to be ≤15°. This assures that the rebound and reentrainment effects at the edge of the inlet face are negligible.

The sampling efficiency of the entire inlet system is defined as

$$E_s = C_s/C_o \tag{1}$$

and may be characterized by the product of three distinct efficiencies (*6*, *7*)

$$E_s = E_a E_r E_t \tag{2}$$

where C_s is the particle concentration after passage through the inlet and C_o is the true particle concentration in the original air environment. The aspiration efficiency, E_a, is the ratio of the particle concentration at the face of the inlet to that in the undisturbed environment. The entry efficiency, E_r, is the ratio of the particle concentration passing the inlet face to that incident to the face. The transmission efficiency, E_t, is the ratio of the particle concentration exiting from the inlet tube to that just past the inlet face, which accounts for the particle losses to the inside wall of the inlet by gravitational settling, impaction, and turbulent or laminar diffusion, depending on the sampling conditions. Because of the thin-walled and sharp-edged design of our inlet, the entry efficiency, E_r, is assumed to be unity, so that

$$E_{s,R} = E_{a,R}E_{t,R} \tag{3}$$

Here, a further subscript is used to show the velocity ratio, R, which is defined as

$$R = U_w/U_i \tag{4}$$

where U_w and U_i are the wind velocity outside the inlet and the average sampling velocity in the inlet, respectively.

In conventional wind tunnel studies the sampling is determined by collecting the sampled aerosol on to a filter

† Present address: Department of Energy Engineering, Toyohashi University of Technology, Tempaku-cho, Toyohashi, 440 Japan.

 0013-936X/87/0921-0178$01.50/0

Table I. Experimental Conditions

parameter	value	no. of combinations
d_{ae}, μm	5–40	5
U_w, cm/s	250, 500, 1000	3
U_i, cm/s	125, 250, 500, 1000	4
D_i(i.d.)		
cm	0.32, 0.56, 1.03, 1.59	4
in.	$^4/_{32}$, $^7/_{32}$, $^{13}/_{32}$, $^{20}/_{32}$	
D_i(o.d.)		
cm	040, 0.64, 1.11, 1.67	
in.	$^5/_{32}$, $^8/_{32}$, $^{14}/_{32}$, $^{21}/_{32}$	
L, cm	20	1
		total = 240

and determining the filter deposit gravimetrically or fluorometrically. The generation of performance curves for a given inlet is generally very time consuming when this conventional technique is used. In our studies we determine the incident aerosol concentration once for each combination of wind and particle generation conditions by sampling isoaxially and isokinetically into the optical single particle counter (OPC) and determining the transmission loss in the inlet body by a fluorescence technique used on uranine-tagged oleic acid aerosol particles (*23*). While monitoring the aerosol generation for continuous and steady particle production, all non-isokinetic data are acquired with untagged particles by optical particle counting and relating the particle count to the upstream aerosol concentration measured at isokinetic conditions. The overall sampling efficiency is thus

$$E_{s,R} = C_{s,R}/C_o = (C_{s,R}/C_{s,1})(C_{s,1}/C_o) = E_{rel,R}E_{s,1} \quad (5)$$

where the relative sampling efficiency, $E_{rel,R}$, is defined as the ratio of the optical particle count at non-isokinetic conditions to the optical particle count at isokinetic conditions. Since the aspiration efficiency is unity for isokinetic sampling

$$E_{s,1} = E_{t,1} \quad (6)$$

the overall sampling efficiency for non-isokinetic conditions is now the product of the relative sampling efficiency dynamically measured by the optical counter and the transmission efficiency at isokinetic conditions:

$$E_{s,R} = E_{rel,R}E_{t,1} \quad (7)$$

The experimental conditions investigated in this study are shown in Table I. The parameters d_{ae}, D_i, and L are the aerodynamic particle diameter, inlet inner diameter, and inlet length, respectively. Of the 240 possible parameter combinations, 210 cases have actually been tested. Thirty combinations for the largest inlet were omitted because the experimental system could not handle the high flow rate in the inlet for the highest wind velocity.

These experimental conditions correspond to a Stokes number, Stk, of 0.01–10 and velocity ratio, R, of 0.25–8, where the Stokes number is defined as

$$\text{Stk} = \tau U_w/D_i \quad (8)$$

and τ is the relaxation time, defined as

$$\tau = \rho_p d_p^2/(18\eta) \quad (9)$$

where ρ_p is the particle density, d_p is the particle diameter, and η is the air viscosity. Relaxation time τ is a measure of how quickly a particle adapts to a change in velocity of the surrounding air (*27*). At least three measurements were performed for each of the 210 parameter combinations in Table I, and their mean value, the standard deviation of

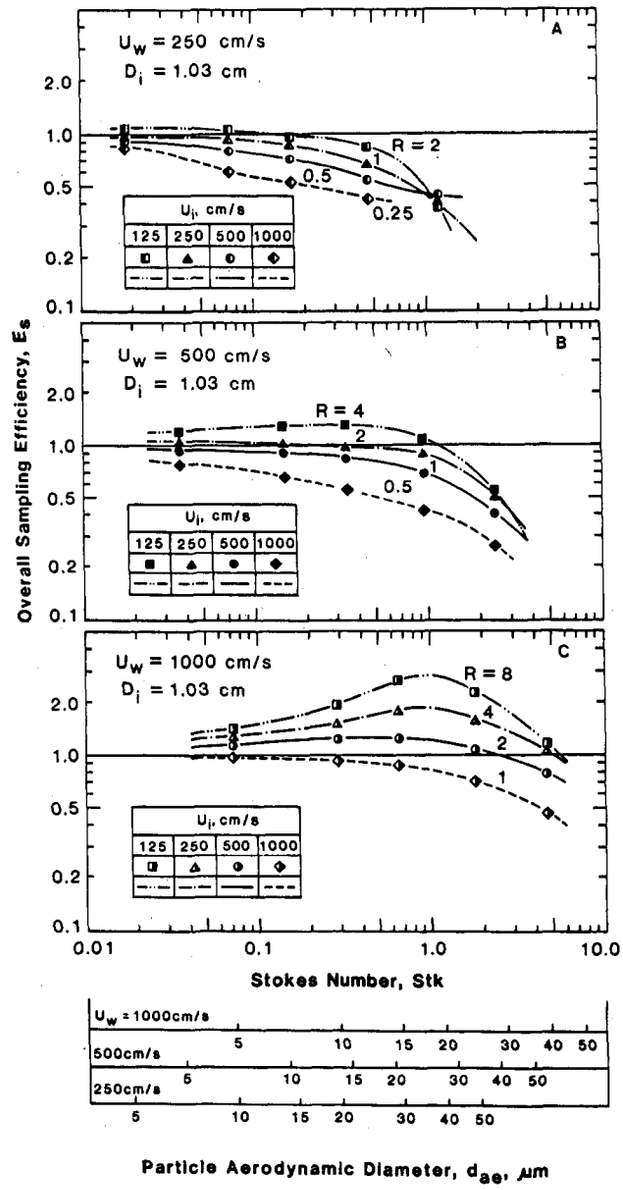

Figure 1. Inlet performance for a fixed inlet diameter: (A) U_w = 250 cm/s; (B) U_w = 500 cm/s; (C) U_w = 1000 cm/s.

which is about 2.0% or less, was used in our data analysis. Only through use of our dynamic measurement technique mentioned above was it possible to perform such a large number of systematic experiments. As a result, a large body of consistent data has been available for the development of our models.

Results and Discussion

Since aspiration efficiency data for given air velocities and particle sizes are generally nondimensionalized (*4–7*) through velocity ratio, R, and Stokes number, Stk, most of our data in Figures 1–8 are presented as a function of Stokes number.

Figure 1 shows all the overall sampling efficiency data obtained for an inlet inner diameter of 1.03 cm. Our data for the other inlet sizes, 0.32, 0.56, and 1.59-cm inner diameters, have similar features when plotted in this manner and are included in subsequent figures. Figure 1 shows as a general tendency that all overall or total sampling efficiency data approach unity as Stokes number tends to zero for which the inertial effect disappears. For Stk < 0.1, the sampling efficiency is 100 ± 10%, and for Stk < 0.03, it is 100 ± 20%. As Stokes number increases, the

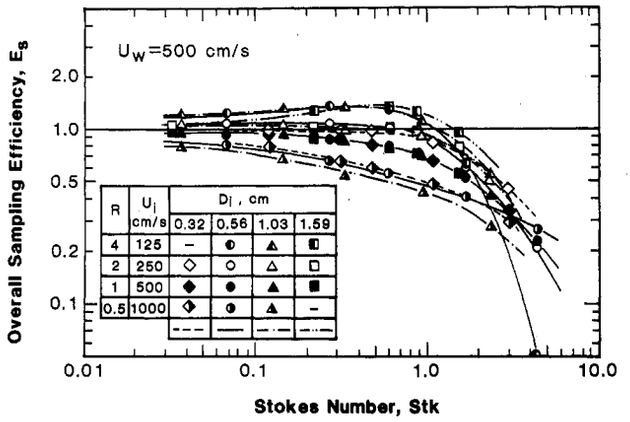

Figure 2. Inlet performance for different inlet diameters, U_w = 500 cm/s.

sampling efficiency curves diverge depending on the velocity ratio and the wind velocity. For sufficiently large Stokes numbers, the overall sampling efficiencies decrease. This could be attributed to particle losses through gravitational deposition inside the inlet. The sampling efficiency decrease is a rather complicated phenomenon. It will be discussed by regrouping the data as shown in the following sections.

The overall sampling efficiency data for a wind velocity of 500 cm/s shown in Figure 1B for different velocity ratios, R, are replotted in Figure 2 with the data for the other three inlet sized added. As seen, the sampling efficiency for a fixed wind velocity is a function of Stokes number and velocity ratio and is not an explicit function of inlet size even in the high Stokes number region. Our data, thus, prove that the effect of inlet size is truely included in the expression for Stokes number although some small deviations appear for extremely large Stokes numbers. Figure 2 shows that the decrease of sampling efficiency at large Stokes numbers is more pronounced for the higher velocity ratios. Figures 1 and 2 both show that the velocity ratio curves cross each other at large Stokes numbers. This crossover occurs because the larger velocity ratios have the lower inlet velocities for a fixed wind velocity. For larger particles, gravitational deposition in the inlet increases, as the ratio of average residence time in the inlet to the time for particle sedimentation increases, thus causing a more pronounced decrease in sampling efficiency at high Stokes number. At lower Stokes numbers, the effect of aspiration controls the overall sampling efficiency. Here, the overall sampling efficiency is higher for the higher velocity ratios. The aspiration efficiency has been studied extensively and may be expressed as (*7*, *11*)

$$E_a = 1 + (R - 1)\frac{2R + 0.62}{R/\mathrm{Stk} + 2R + 0.62} \qquad (10)$$

For the other wind velocities of 250 and 1000 cm/s, the tendencies are similar to the ones shown in Figure 2.

If an aerosol in a specific wind environment is to be sampled at a specific velocity, one may ask which inlet size should be chosen. Figure 3 explicitly shows the effect of inlet size on the sampling efficiency for two air velocity combinations (R = 1 and 2). In order to show the effect on the given particle size distribution, the performance curves are plotted as a function of aerodynamic diameter. Figure 3 shows that, in general, the maximum possible inlet diameter should be chosen for the optimal sampling efficiency. At smaller inlet diameters, particle deposition in the inlet is higher, resulting in reduced sampling efficiencies.

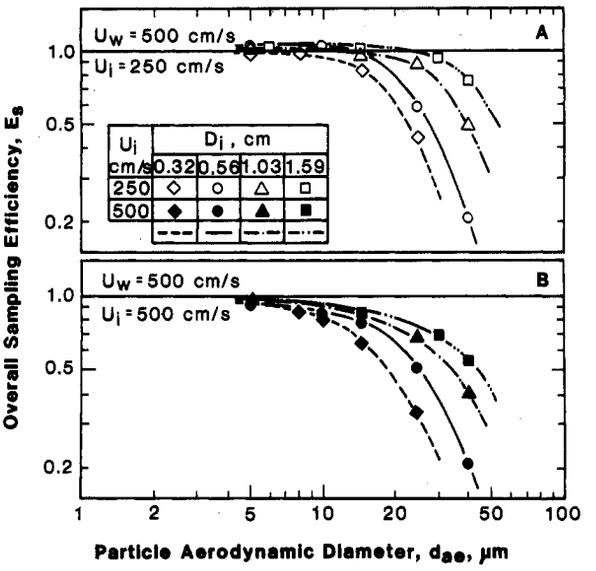

Figure 3. Overall sampling efficiency vs. aerodynamic particle diameter for a wind velocity of 500 cm/s: (A) U_i = 250 cm/s; (B) U_i = 500 cm/s.

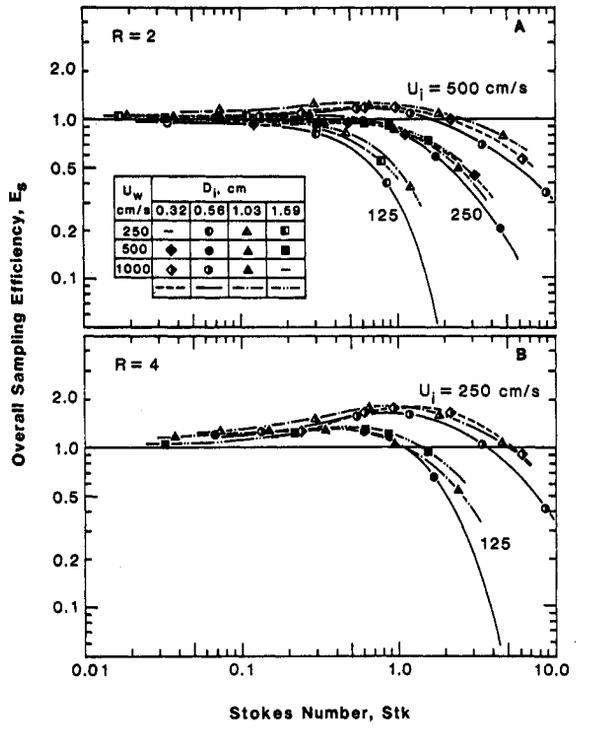

Figure 4. Inlet performance for fixed velocity ratios: (A) R = 2; (B) R = 4.

Data presentation with different parameters fixed generally illustrates different features of the process under study. Figure 4 shows overall sampling efficiency data plotted for fixed velocity ratios. While the data shown in Figures 1 and 2 converge to common efficiency values for Stk < 0.03, when presented for fixed wind velocities, we find from Figure 4 that the same data show uniform behavior for Stokes number up to about 0.3, essentially independent of inlet size and inlet velocity, when plotted for fixed sampling ratios. In the Stokes number region of 0.03 < Stk < 0.3, the overall sampling efficiency deviates from unity by the aspiration effect, but the deposition effect in the inlet is still not very significant. For larger values of Stokes number, particle losses by deposition in the inlet become dominant, and lower overall sampling efficiencies are attained for smaller wind and inlet velocities.

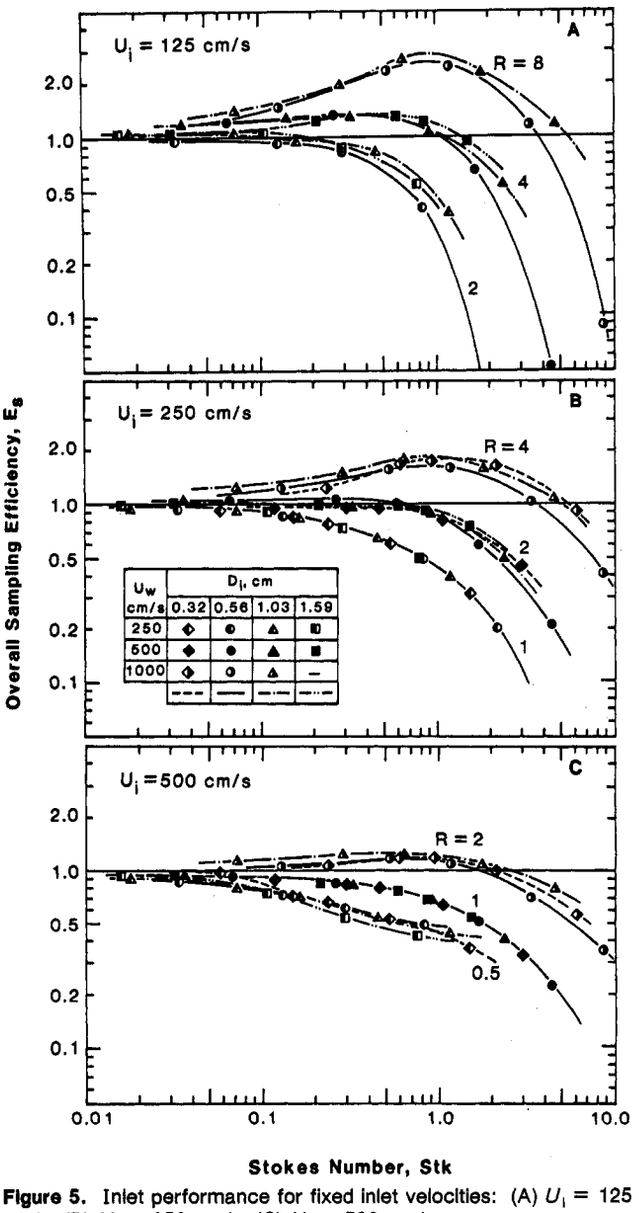

Figure 5. Inlet performance for fixed inlet velocities: (A) U_i = 125 cm/s; (B) U_i = 250 cm/s; (C) U_i = 500 cm/s.

The inlet velocity is considered to be the most important fluid dynamic parameter controlling the transmission or deposition phenomena in the inlet. The results for fixed inlet velocities of 125, 250, and 500 cm/s are shown in Figure 5 in order to demonstrate the effect of R, the ratio of U_w/U_i, independent of inlet velocity. Even though each individual panel includes data from four different inlets, as in Figure 2, the effect of inlet size is now well represented as a function of Stokes number, and the data for given U_i and R values plot smoothly. For the large Stokes number region, though, the rate of decrease in overall sampling efficiency is much greater for the smaller inlet velocity, but the shapes of the decreasing portions of the curves are similar to each other in each panel with a fixed inlet velocity. This suggests that the decrease in overall sampling efficiency by particle losses in the inlet should be plotted as a function of a new parameter that represents all of the flow and particle behavior in the inlet.

A study of the transmission losses in our inlets has shown that the performance curves can be represented by a combination of three nondimensional parameters. We define inlet deposition parameter K as

$$K = [(Z \times \mathrm{Stk})/\mathrm{Re}^{1/2}]^{1/2} \tag{11}$$

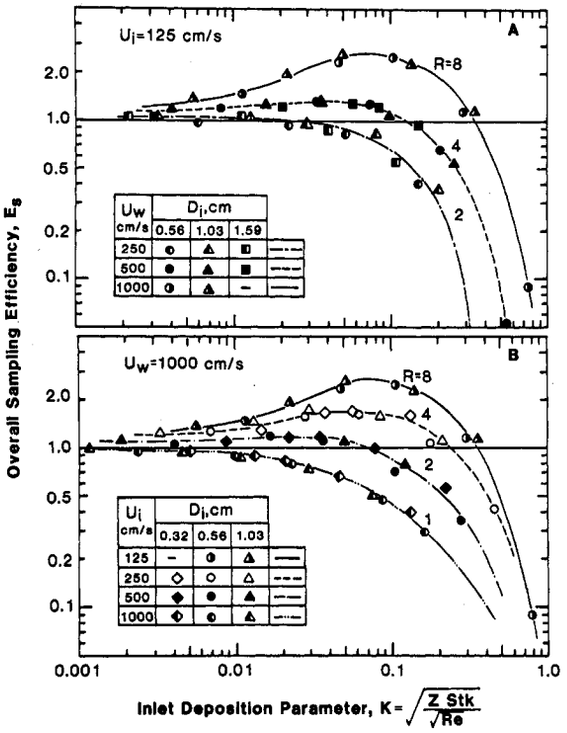

Figure 6. Inlet performance as a function of inlet deposition parameter K: (A) U_i = 125 cm/s; (B) U_w = 1000 cm/s.

which includes the effects of particle inertia, particle entrainment in the developing boundary layer inside the inlet, and gravitational deposition of particles on the inner wall.

In this expression, Z and Re are the gravitational deposition parameter (*27*, *28*) and Reynolds number (*29*), respectively, defined by

$$Z = (L/U_i)/(D_i/V_s) \tag{12}$$

$$\mathrm{Re} = U_i D_i/\nu \tag{13}$$

where V_s is a gravitational settling velocity (*27*) and ν is the kinematic viscosity of air. Utilizing this new parameter, the transmission efficiency for isoaxial sampling with different sized inlets is represented by

$$E_{t,R} = \exp(-4.7K^{0.75}) \tag{14}$$

The coefficient and exponent in this equation have been determined empirically by a best-fit procedure.

Figure 6 shows the measured sampling efficiencies plotted as a function of inlet deposition parameter, K. If we fix the inlet velocity, Figure 6A, as we already did in Figure 5, the decreasing portions of the sampling efficiency curves at the higher K values are now congruent; i.e., their shapes are similar to each other. The effect of aspiration is still seen in the middle range of inlet deposition parameter, K. In Figure 6B the wind velocity is fixed at 1000 cm/s. All of the overall sampling efficiency curves now approach zero at K values just below 1, in spite of their differences in inlet velocities. These results show that the new parameter K expresses well isoaxial sampling and transmission of high Stokes number particles through tubular inlets facing the wind in the horizontal direction.

We have presented comprehensive data for the overall or total sampling efficiencies of inlets. For the thin-walled and sharp-edged inlets used, the overall sampling efficiency has been described as the product of aspiration efficiency and transmission efficiency (see eq 3). Since aspiration efficiency has been studied extensively, we can now

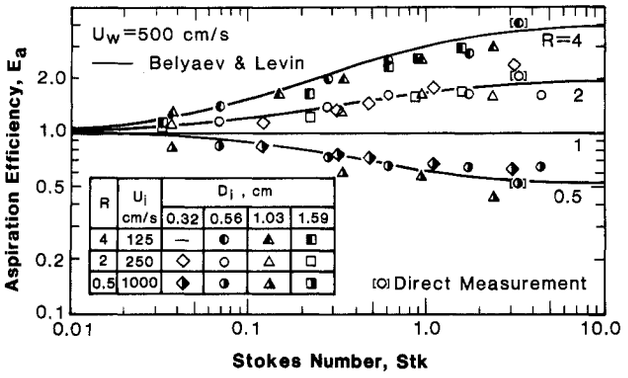

Figure 7. Aspiration efficiency vs. Stokes number, calculated from the measured overall sampling efficiencies; U_w = 500 cm/s.

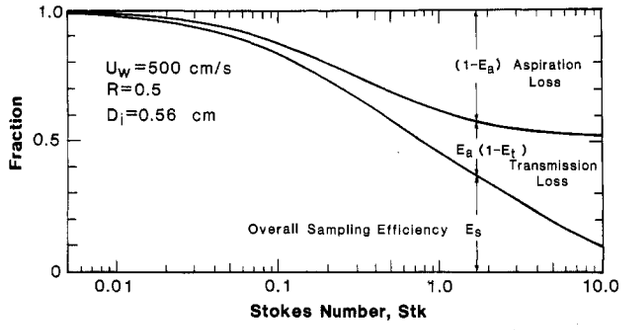

Figure 8. Relative contributions of aspiration and transmission losses to overall sampling efficiency.

backcalculate the aspiration efficiency from our total sampling efficiency values, E_s, and our transmission efficiency values, E_t, given by eq 14. The aspiration efficiencies thus obtained are shown in Figure 7 for the case of U_w = 500 cm/s. As seen, they agree very well with the solid lines given by eq 10, which are widely accepted to express the aspiration efficiency (*11*, *27*). This good agreement suggests that the combination of the expressions for E_a in eq 10 and E_t in eq 14 may be applied not only to estimate the overall sampling efficiency but also to discriminate the dominant causes that modify the aerosol concentration during sampling. Figure 8 shows an example for U_w = 500 cm/s, D_i = 0.56 cm, and R = 0.5. This figure clearly shows which mechanism dominates in reducing the particle concentration and to what extent aspiration and transmission losses affect the concentration measured by a sensor downstream of the inlet.

Conclusions

The following conclusions result from our experimental study on the sampling efficiency of thin-walled, sharp-edged inlets sampling isoaxially from horizontal airflows under laminar flow conditions.

(1) Losses of large aerosol particles by gravitational deposition in the inlet increase with decrease of inlet diameter.

(2) In the small Stokes number region, the overall sampling efficiency is 100 ± 10% for Stk < 0.01 and 100 ± 20% for Stk < 0.03. For 0.03 > Stk < 0.3, the overall sampling efficiency is expressed well as a function of Stokes number with velocity ratio as a parameter.

(3) In the larger Stokes number region, Stk > 0.3, particle losses in the inlet significantly reduce the overall sampling efficiency. Here, the inlet performance is characterized well by a new inlet deposition parameter, K, eq 11, which is a combination of nondimensional Stokes number, gravitational deposition parameter, and Reynolds number.

(4) Aspiration efficiencies calculated from the measured overall sampling efficiencies, E_s, eq 3, and the measured transmission efficiency, E_t, eq 14, agree well with the predicted values for aspiration efficiency, eq 10.

(5) Overall sampling efficiencies and the dominant causes that modify the aerosol concentration can be calculated from the expressions for aspiration efficiency, eq 10, and the transmission efficiency, eq 14.

Acknowledgments

We thank Morris S. Ojalvo of NSF for his efforts and support. We appreciate the help of Alex Fodor in building the wind tunnel facility at the University of Cincinnati.

Literature Cited

(1) Davies, C. N. *Staub—Reinhalt. Luft (Engl. Transl.)* **1968**, *28*(6), 109.
(2) Watson, H. H. *Am. Ind. Hyg. Assoc., Q.* **1954**, *15*, 21–25.
(3) Levin, L. M. *Bull. Acad. Sci. USSR, Geophys. Ser.* **1957**, 7(Part II), 87–101.
(4) Badzioch, S. *Br. J. Appl. Phys.* **1959**, *10*, 26–32.
(5) Lundgren, D. A.; Calvert, S. *Am. Ind. Hyg. Assoc. J.* **1967**, *28*, 208–215.
(6) Belyaev, S. P.; Levin, L. M. *J. Aerosol Sci.* **1972**, *3*, 127–140.
(7) Belyaev, S. P.; Levin, L. M. *J. Aerosol Sci.* **1974**, *5*, 325–338.
(8) Yoshida, H.; Ohsugi, T.; Masuda, H.; Yuu, S.; Iinoya, K. *Kagaku Kogaku Runbunshu* **1976**, *2*(4), 336–340.
(9) Selden, M. G. *J. Air Pollut. Control Assoc.* **1977**, *27*, 235–236.
(10) Davies, C. N.; Subari, M. B. *Proceedings of Advances in Particle Sampling and Measurement*; U.S. Environmental Protection Agency. U.S. Government Printing Office: Washington, DC, 1979; U.S. EPA 600/7-79-065, pp 1–29.
(11) Durham, M. D.; Lundgren, D. A. *J. Aerosol Sci.* **1980**, *11*, 179–188.
(12) Jayesekera, P. N.; Davies, C. N. *J. Aerosol Sci.* **1980**, *11*, 535–547.
(13) Davies, C. N.; Subari, M. *J. Aerosol Sci.* **1982**, *13*(1), 59–71.
(14) Sehmel, G. A. *Am. Ind. Hyg. Assoc. J.* **1970**, *31*, 758–771.
(15) Ogden, T. L.; Birkett, J. L. *Ann. Occup. Hyg.* **1978**, *21*, 41–50.
(16) Pattenden, N. J.; Wiffen, R. D. *Atmos. Environ.* **1977**, *11*, 677–681.
(17) Wedding, J. B.; McFarland, A. R.; Cermak, J. E. *Environ. Sci. Technol.* **1977**, *11*, 387–390.
(18) Liu, B. Y. H.; Pui, D. Y. H. *Atmos. Environ.* **1981**, *15*, 589–600.
(19) Vrins, E.; Hofschreuder, P. *J. Aerosol Sci.* **1983**, *14*, 318–322.
(20) Wedding, J. B.; Carney, T. C. *Atmos. Environ.* **1983**, *17*, 873–882.
(21) Mark, D.; Vincent, J. H.; Gibson, H.; Lynch, G. *Am. Ind. Hyg. Assoc. J.* **1985**, *46*, 127–133.
(22) Wedding, J. B.; Weigand, M.; John, W.; Wall, S. *Environ. Sci. Technol.* **1980**, *14*, 1367–1370.
(23) Tufto, P. A.; Willeke, K. *Environ. Sci. Technol.* **1982**, *16*, 607–609.
(24) Tufto, P. A.; Willeke, K. *Am. Ind. Hyg. Assoc. J.* **1982**, *43*, 436–443.
(25) Tufto, P. A. Ph.D. Dissertation, University of Cincinnati, Cincinnati, OH, 1981.
(26) Berglund, R. N.; Liu, B. Y. H. *Environ. Sci. Technol.* **1973**, *7*, 147–153.
(27) Hinds, W. C. *Aerosol Technology*; Wiley: New York, 1982; Chapter 5.
(28) Schwendiman,L. C.; Stegen, G. E.; Glissmeyer, J. A. Report BNWL-SA-5138; Battelle Pacific Northwest Laboratory: Richland, WA, 1975.
(29) Schlichting, H. *Boundary Layer Theory*, 4th Ed.; McGraw-Hill: New York, 1960; Chapter 2.

Received for review March 14, 1986. Accepted September 19, 1986. This material is based upon work supported by the U.S. National Science Foundatation under Grant CPE-8213269.